NDE2002 predict. assure. improve.
National Seminar of ISNT
Chennai, 5. – 7. 12. 2002
www.nde2002.org

# NDT - Techniques for Life Time Assessment of Components In Service – An International Cooperative Approach

**N.P. Aleshin*, I. Altpeter**, G. Dobmann**, M. Kroening**, A. Reddy*****

*Moscow Bauman State Technical University, Russia,
**Fraunhofer Institute for NDT, Saarbruecken, Germany,
***QNET Ltd, Chennai, India, dobmann@izfp.fhg.de

**Abstract**:

Service induced degradation of material properties is the main limiting factor for the operating life time of components and structures such as pressure vessels and pipelines. Degradation of the mechanical properties of reactor pressure vessel material includes for example a decrease in fracture toughness, an increase in strength and in the fracture appearance transition temperature (FATT). We discuss and verify by SANS-experiments the effects of operating factors on intrinsic material properties (microstructure) that affect properties, which can be measured by NDT techniques. We demonstrate the potential of electromagnetic techniques for characterization mechanical strength that is based on the correlation between dislocations and domain wall movement. The discussed material is the low-alloy, heat resistant WB 36 (15 NiCuMoNb 5). A measurement system was successfully calibrated for the prediction of HV 10 by Barkhausen noise measurement and upper harmonics analysis of the magnetic field. The applicability of this approach was investigated by proving its independence on side-effects like plastic deformation and tensile load. Early fatigue damage and thus remaining lifetime of austenitic stainless steel is correlated to changes of the magnetic permeability and electrical conductivity, which is discussed and described by experiments. For on-line fatigue monitoring of austenitic stainless steel components a GMR sensor technique is proposed and demonstrated. Furthermore, a new thermal NDE method for fatigue damage characterization of Ti 6Al 4V will be presented, which is based on dissipated heat evaluation.

## 1. Introduction

Service induced degradation of reactor pressure vessels according to licensing regulations is the main limiting factor of the operating life time of nuclear power plants. Degradation of reactor pressure vessel material properties includes a decrease in fracture toughness, an increase in strength and an increase in the fracture appearance transition temperature (FATT). The vessel operating factors, primary neutron irradiation and thermal ageing, have an effect on intrinsic material properties (microstructure) that affect both mechanical and electromagnetic properties. The magnetic and electrical properties influence electromagnetic NDT quantities that may be used to monitor the condition of reactor pressure vessel materials in so far as NDT results reliably correlate with mechanical properties and relevant components are accessible.

In German power plants the copper-alloy ferritic steel WB 36 is used for piping material below an operating temperature of 300°C and for vessel material up to an operating temperature of 340°C. Over the last 10 to 15 years failures to components made of WB 36 have arisen in conventional power plants after long-term operation. Smallest operating-induced copper precipitates with a particle diameter of 1.5 to 3.0 nm can cause material degradation which results in decrease in toughness and an increase in the fracture appearance transition temperature [1]. An example for such damage is a feed water pipe of WB 36 which exploded after 130,000 operating hours at 350° C in the conventional power plant Kardia 1 in Greece in 1998 [2].

The evaluation of early fatigue damage and thus the prediction of the remaining lifetime is a task of practical relevance for example in the chemical, nuclear, as well as in the

aircraft industry. High performance material e.g. titanium is used in aircraft structures. Especially under high-cycle fatigue conditions more than 90% of lifetime is spent before cracks are usually detectable. The reasons for this are small cracks and subsurface cracks generated from fatigue induced compressive stresses within the surface region. Under HCF conditions very small non-detectable cracks can become unstable and result in catastrophic failure.
In the chemical industry, for example, austenitic stainless steels are in widespread use, mainly because of their high toughness and resistance to corrosion attack. However, under static as well as fatigue load the material has the tendency to respond with localized phase transformation from the non-magnetic $\gamma$ to the martensitic and ferromagnetic $\alpha'$ phase. Magnetic permeability changes are observed in the martensitic structure development and in residual stress effects where the electrical conductivity is influenced by the changing dislocation density and arrangement. Bearing in mind the tasks faced by industry with regard to titanium and austenitic stainless steels, new approaches to on-line monitoring of fatigue characterization are essential.

## 2. Characterization of material degradation

2.1 NDE of material degradation caused by embrittlement

In the framework of a research project [1], a very extensive microscopic characterization of the WB 36 material was performed by Karl-Heinz Katerbau and his group at the University of Stuttgart. The microstructure was investigated with the aid of SANS (Small Angle Neutron Scattering), appropriate for the detection of smallest Cu-precipitates as well as with TEM (Transmission-Electron-Microscopy) suitable for the detection of larger Cu-precipitates. SANS investigations have proved that globular Cu-particles in the range of 1-3 nm are responsible for the decrease in toughness. Larger coherent particles (> 3 nm) are characterized in the TEM by the coffee-bean–like shape as shown in Fig. 1.

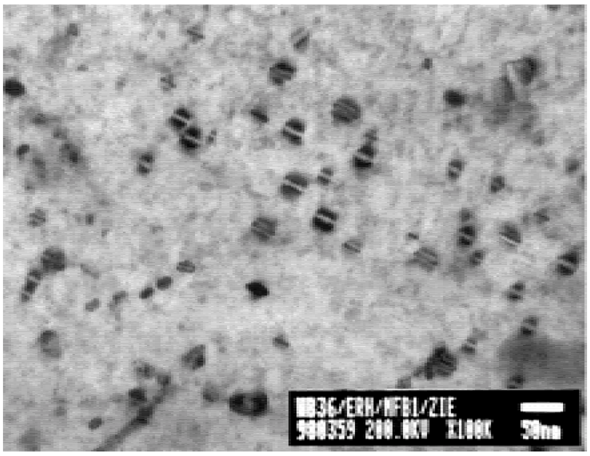

**FIGURE 1** WB-36-Cu-precipitations after long-term service

At the IZFP an approach has been developed for the determination of residual stresses of the third order, i.e. residual stresses of coherent precipitates [3]. The procedure is based on the load dependent Barkhausen analysis and allows a determination of residual stresses with an accuracy of ± 1.5 MPa. On the basis of this procedure measurements were carried out on service exposed and recovery-annealed specimens originating from a vessel drum of WB 36.[4]
Between both microstructure states a residual stress difference of about 20 MPa was determined. This value is small because it is an integral value. The local residual stress state in the vicinity of a copper precipitate is much higher and can be in the yield strength range.

Investigations by MPA Stuttgart have shown that Vickers hardness is suitable for the quantification of embrittlement though it has the disadvantage that it is not repetitively and area–wide applicable and because spot tests require information about critical test areas. Non-destructive early-detecting of the hardness increase is therefore a most favorable solution for this problem. Based on the analogy between dislocation and Bloch-wall movement, electromagnetic measuring techniques are suitable for the determination of mechanical material properties. The suitability of micro-magnetic NDE techniques for the characterization of the Vickers hardness was investigated. A measuring system was successfully calibrated for the prediction of HV 10 by Barkhausen noise and upper harmonics analysis of the magnetic field. Electromagnetic measurements and Vickers hardness measurements were carried out on 12 cylindrical samples which were service-simulated at a temperature of 400° C. All investigated samples reveal a hardness maximum after 1,000 h length of service simulation. The mean increase in hardness is about 40 HV 10. The decrease in the hardness after passing through a maximum is caused by the growth of copper precipitates, the so-called "Ostwald-Ripening" [5].

Fig.2 shows the magnetic hardness, i.e. a coercivity $H_{co}$, in comparison with the mechanical hardness, HV 10, as function of length of service simulation.

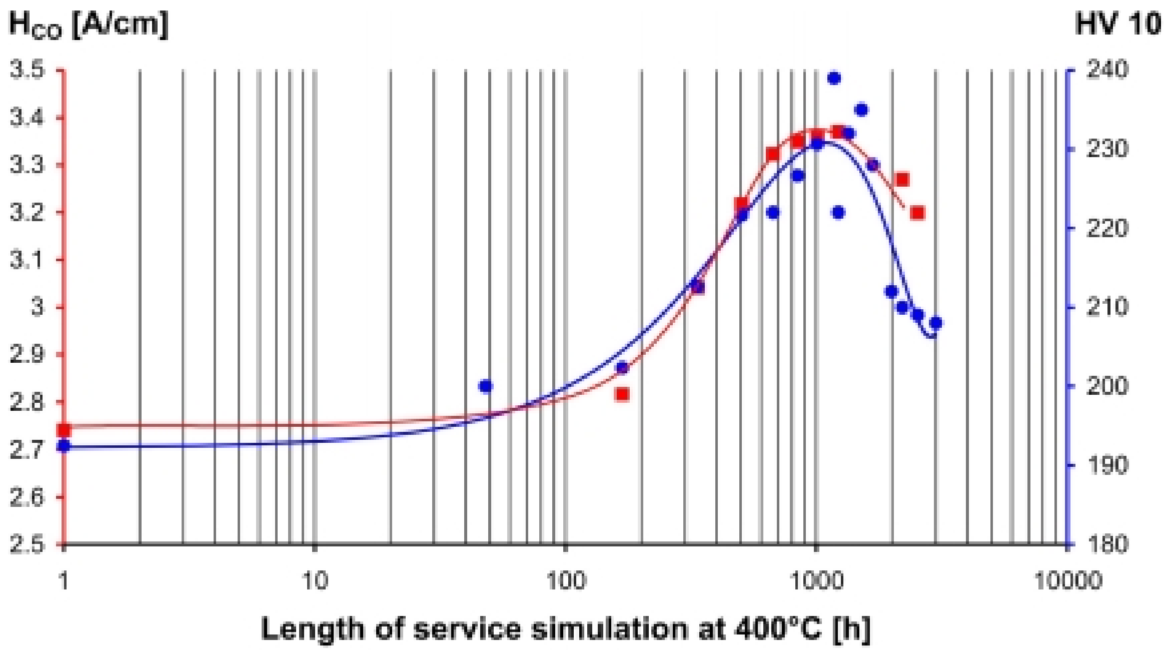


**FIGURE 2** Coercivity values $H_{CO}$ [■] in comparison with HV 10 values [●] as function of length of service simulation at 400°C [h].

Fig.3 demonstrates the sufficiently good correlation between non-destructively determined hardness values and mechanical hardness values. The correlation coefficient was better than 0.97 and the error band was smaller than 5 HV 10. In order to prove the practicability of this approach, it was also tested under superimposed tensile loads in order to simulate residual stress influences. The electromagnetic hardness determination succeeds even under such unfavorable outside influences.

Parallel to the activities in Germany in 1999 within the framework of a research program from the Nuclear Regulatory Commission, Donna Hurley at the National Institute of Standards and Technology has carried out non-linear ultrasonic measurements on A710 steels with copper-rich precipitates [6]. The behavior of this steel is similar to that of WB36, although there are minor differences in their respective chemical compositions [6]. The measuring quantity derived from non-linear ultrasonic measurements is the non-linearity factor ß [6].

$$\beta = {(8A_2)}\Big/{(A_1^2 k^2 L)} \qquad (1)$$

In (1) k = ($2\pi/\lambda$), the wave number, L is the sound-path length, A1 is the amplitude of the fundamental and A2 the amplitude of the first of the higher harmonics.

The non-linearity parameter β was compared with Vickers hardness values. According to Donna Hurley the reason for the deviation is the influence of internal coherency strains surrounding the precipitates on the parameterβ.

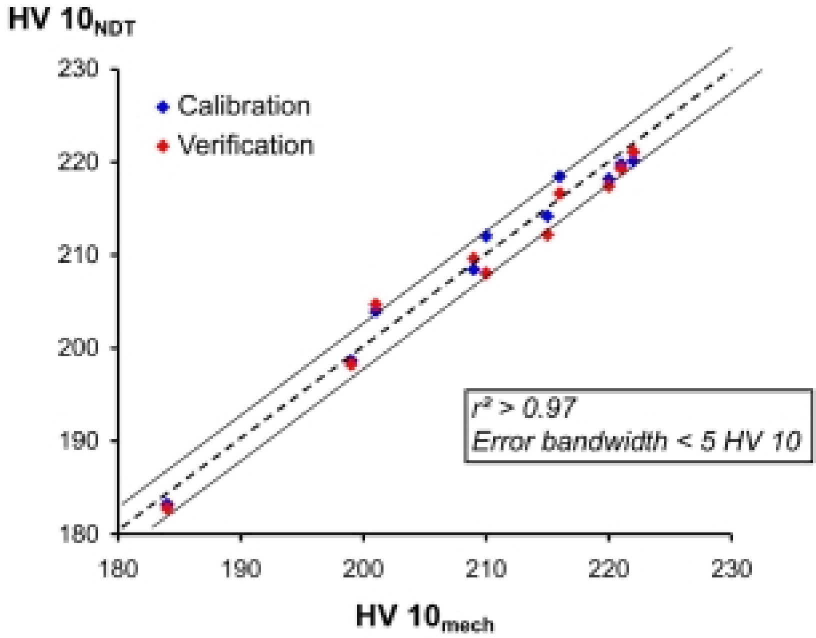


**FIGURE 3** Correlation between non-destructively predicted hardness values (HV $10_{NDT}$) and Vickers hardness values (HV 10 mech), correlation coefficient $r^2 > 0.97$, and error bandwidth < 5 HV 10.

Reactor pressure vessel steels contain only a third of the copper content of WB 36. However, also in this case**,** the embrittlement is caused by copper rich precipitates as a consequence of neutron irradiation. At the IZFP, electromagnetic measurements were carried out on different neutron irradiated samples by using the micro-magnetic 3MA device [7[.

In a hot cell laboratory with a manipulation system, electromagnetic measurements were performed on irradiated Charpy-V samples from the Chinon nuclear power plant in France. 5 pairs of samples with different exposure times (0, 4, 7, 9, 14 years) were investigated. Calibration was performed on the base of only 5 of the samples; one measurement of each exposure time was made, using the fluence value as reference value. Good correlation (R=0.98) was obtained between fluence predicted by 3MA and fluence reference values by testing the approach with the remaining 5 specimen.

George Alers at The National Institute of Standards and Technology in Boulder, USA, carried out dynamic magnetostriction measurements by using EMATs on a CT-sample set which was neutron irradiated inside a hot cell. A correlation was found between the phase velocity of the magnetostrictively excited shear wave and the neutron irradiation. However, the technique cannot be applied at the pressure vessel component, where the highest degree in embrittlement has to be expected in the cladding-near material zones in the ferritic vessel material. Therefore, by the development of a NDE technique for determination of embrittlement in an installed reactor pressure vessel the stainless steel cladding on the inside surface of the vessel has to be taken into consideration. This layer is about 10 mm thick and can complicate the penetration of the cladding by using magnetic fields and ultrasonic waves.

The first successful measurement on a pressure vessel section with a 10 mm thick cladding was performed by George Alers. A pair of permanent magnets and an electromagnet has been used for exciting an ultrasonic shear wave by magnetostrictive coupling in the ferromagnetic base material. The frequency of this shear wave was the same as that used to drive the electromagnet, about 10 kHz. This low frequency was applied for an adequate penetration of the cladding and producing a thickness resonance with respect to the wall thickness. Whereas the resonance frequency is determined by the wall thickness which locally can change, the resonance amplitude is strongly influenced by the magnetostriction value of the cladding-near zones in which the wave is excited. Magnetostriction uniquely changes with embrittlement.

## 2.2 NDE of material degradation caused by fatigue

Cyclic loading leads to heat dissipation caused by internal friction and micro-plasticity. Excitation of this thermal effect within the specimen was achieved in a servo hydraulic fatigue machine and temperature measurements were made using an infrared camera.

At low cycling frequencies, three stages of the temperature evolution can be observed. Measured after an approximately linear increase of the temperature at the beginning (stage 1), the slope of temperature development with time, dT/dt, decreases gradually (stage 2) due to heat losses (heat conduction, radiation and convection). Finally, an equilibrium temperature is reached, when the heat generation is balanced by the heat losses to the environment (stage 3). This equilibrium temperature has been mostly used for the characterization of fatigue because it depends on the dissipated heat energy which is connected with the area under the mechanical hysteresis. However, the thermal boundary conditions also have a strong influence. In a new approach $\Delta\tau_{diss}$ was measured, which is defined as the temperature change per mechanical loading cycle during stage 1, i.e. it describes the initial slope of the temperature increase. $\Delta\tau_{diss}$ does not depend on the thermal boundary conditions because of the adiabatic behavior during the early stages of the loading. The “thermo damping” approach [8] was performed in order to develop potential for reliable aircraft component monitoring. It offers the capability of rapid, non contact, high resolution characterization applicable for technical components. For the thermal measurement the fatigue experiment was interrupted and after cooling down the titanium specimen was subjected to a short-term mechanical loading of approximately 90 cycles at higher frequency cycling. From the temperature evolution $\Delta\tau_{diss}$ was calculated (Fig. 4).

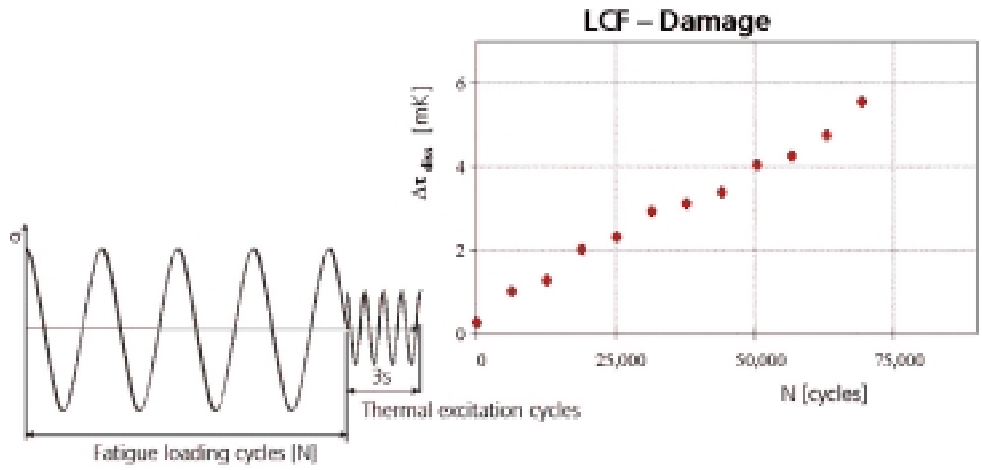


**FIGURE 4** schematic loading sequences: Fatigue loading interrupted by short-term thermal excitation loading cycles. $\Delta\tau_{diss}$ after each block of 6500 fatigue cycles, according to [8].

The monotonic increase of $\Delta\tau_{diss}$ with the number of loading cycles indicates that $\Delta\tau_{diss}$ is a suitable measuring quantity to characterize fatigue.

For characterizing the fatigue behavior of austenitic stainless steel a giant magnetic resistor (GMR)-sensor [9] was used. The GMR was controlled by standard eddy-current equipment. In this experimental set-up an electromagnetic yoke is used as a transmitter coil and the GMR as the receiver. Fig. 5 shows a cyclic deformation curve $\varepsilon_{a,p}$ as function of the load cycles obtained at room temperature and at a load of 380 MPa (stress-controlled experiment).

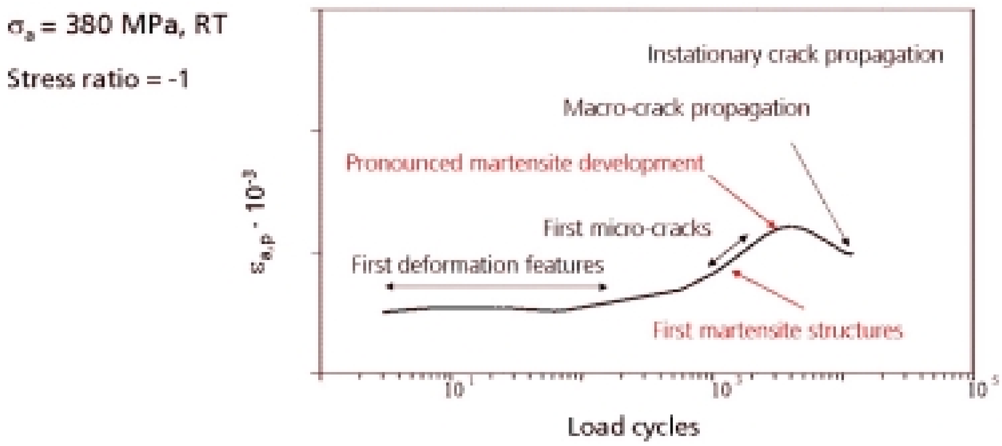


**FIGURE 5** Cyclic Deformation Curve of Steel 1.4541 at Room Temperature (RT).

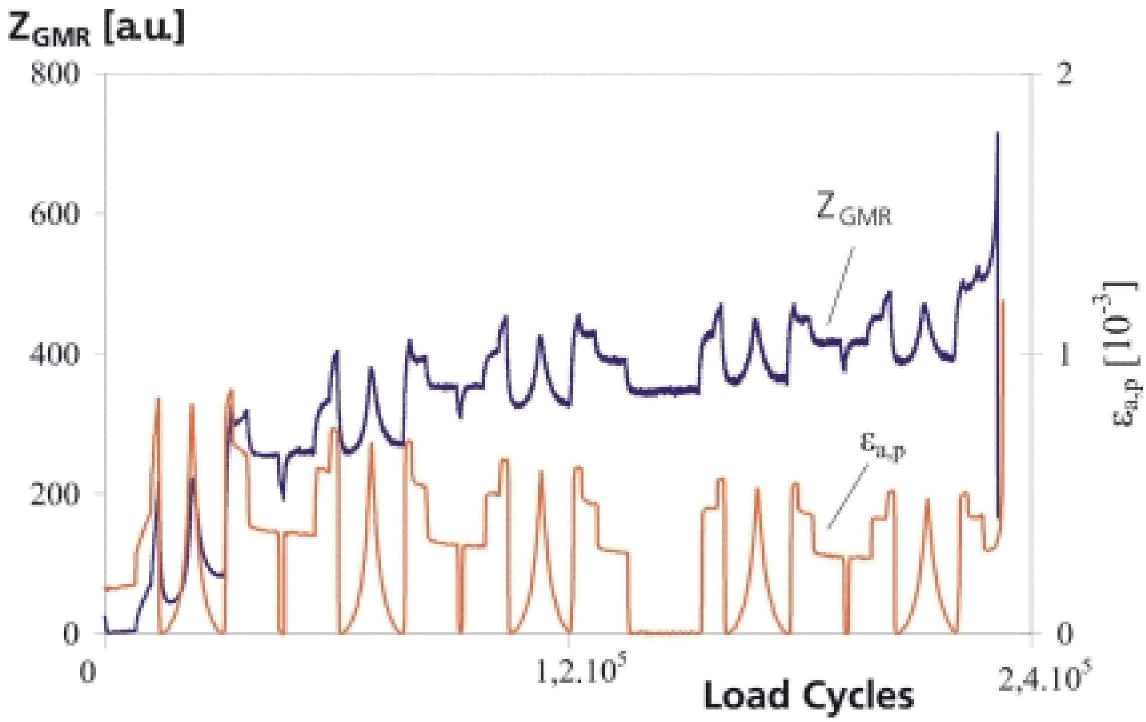


**FIGURE 6** GMR-Transfer-Impedance and Plastic Strain Amplitude for a Multiple Step Load Mix at the Steel 1.4541.

Plastic deformation occurs from the start. First of all, slip lines and Lüders bands are observed in the austenitic phase. With the onset of cyclic softening, first of all martensite structures occur followed by micro-cracks in the austenite and enhanced martensite development after a thousand cycles. With the beginning of the secondary hardening (five thousand cycles), the increase of the martensite phase transformation is pronounced. Extrusions and intrusions occur and macro-crack propagation starts after ten thousand cycles combined with strong failure localization. The martensitic structure development and residual stress effects influence the magnetic permeability. The electrical conductivity is influenced by the changing dislocation density and arrangement. Both effects lead to changes in the GMR-impedance. In stress-controlled fatigue tests the eddy current-impedance measured by the GMR-sensor was found to be especially suitable to characterize the fatigue behavior. Fig.6 is an example of a multiple step fatigue test with a load mix of different amplitudes and time dependencies. The impedance clearly shows an average continuous increase due to the martensite development. The impedance curve is modulated with a time function which follows the plastic strain amplitude exactly, an effect which is assumed to be induced by load and residual stresses. The GMR-technique provides the possibility of on-line, non-destructive characterization of the cyclic deformation behavior of the austenitic steel [10].

## 3. Lifetime assessment after crack appearance

Depending on the component design, the used material, and its degradation state, it is obvious that a component under critical load fails by following a behavior in between the brittle or the ductile regime [11]. In all cases when the material fracture toughness is sufficiently high enough, lifetime consumption by crack initiation and crack growth covers an essential part of the last third of the lifetime before fracture. So far as a reliable crack-sizing NDT-technique exists, NDE can be performed in in-service inspection strategies with adopted inspection periods. These have to be selected such that critical crack growth cannot be overseen. The evaluation then is on the base of fracture mechanic approaches and critical engineering assessment [12], [13] or in case of LCF or HCF on the base of a Basquin respectively a Manson Coffin rule. The airplane industry takes principal credit of that material behavior by using 'damage tolerance principles' for design [14]. However, other industries where safety-relevant components are employed increasingly adopt the concepts. One successful NDE application in India concerning lifetime management of a fertilizer vessel is following that strategy.

### Crack sizing during Plant Operation

An internal crack had developed in a pressure vessel which was detected by ultrasonics. Since the test had to be done during operation of the plant, high temperature probes had to be used. UT in Pulse-Echo mode as well as manual TOFD, and manual orbital scanning using 45 and 60 degree probes allowed sizing of the crack.

A crack depth b = 7 mm and crack length (on the inner face) 2a = 75 mm was found during the first inspection and after 35 days of continued operation the crack depth b = 7 mm and crack length 2a = 83 mm was measured The crack was located near a circumferential weld joint, the crack plane was perpendicular to the axial direction of the vessel. The cylindrical pressure vessel had an inner diameter of ID = 2700 mm and wall thickness t = 117 mm.

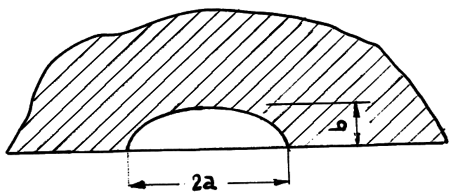

Crack Geometry on ID of the vessel

## Evaluation of Crack with respect of Safety

The assessment of the pressure vessel condition and a judgment on the safety of its operation required more knowledge about the material as well as the operating conditions in order to use fracture mechanics concepts to evaluate the severity of the defect. [19]

## Operating conditions

The pressure vessel had experienced about 48,000 hours of operation, with 56 shut downs. Further the following operational data could be established. Internal pressure under various circumstances is: Steady operation pressure: $P_n$ = 143.2 bar, Maximum operation pressure $P_{max}$ = 146.1 bar, design pressure $P_d$ = 152 bar and Proof test pressure $P_f$ = 197.2 bar. Temperature: on outside wall face 170 ± 15 ºC; on inside wall face approx. 220 ºC.

The composition of the medium inside ammonia converter consists of a mixture of NH3 (4.1-16.6%), H2 (65.92-55.83%), N2 (21.98-18.61%), Ar+CH4 (8.00-8.96%) and Oxygen equivalents max 2 ppm at gas inlet. The outlined limits are related to gas inlet and gas outlet, respectively

**Material and Strength Values**

The construction material was ASTM A384 Gr.22 (12CrMo910Vd), having an ultimate tensile strength (UTS) of 460 MPa and a yield point (YP) of YP = 359 MPa; Heat treatment condition, quenched + tempered + stress relieved at 370 ºC.. While these values were available on the actual material, for fracture toughness $K_{IC}$, the value of static fracture toughness $K_{IC}$ has been assumed at a lower "worst case" value on $K_{IC}$ vs. temperature envelope, according to ASME Pressure Vessel Code (see ASME Sect. XI, App. A and for comments, Marsdon T.U. in EPRI NP-719-SR/1978. A value of KIC = 60 MPa $m^{1/2}$ has been adopted under the conservative assumption that at operation temperature the material display a low fracture toughness that is specific in the nil-ductility transition temperature (T-RTNDT = 0) range. By this assumption a due account has been given to material embrittlement owing to aging and active process environment effects.

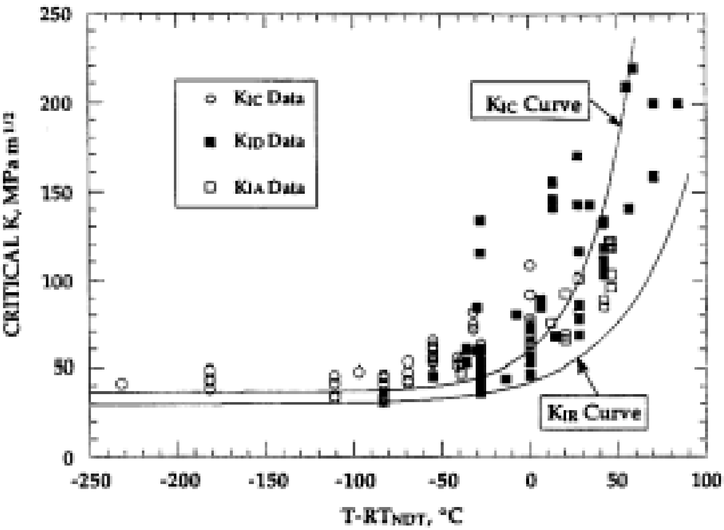


**Failure Risk Assessment ( R6 Procedure Option 1)**

The analysis is based on the concept of the Failure Assessment Diagram (FAD) developed for describing the interaction between fracture and plastic collapse. This methodology is formalized in the R6 Procedure. This procedure enables several options of analysis according to the extent of knowledge concerning strength and fracture mechanics characteristics of the involved material. In the case that only general strength characteristics are known (e.g. UTS, YP, etc.) Option 1 applies. According to R6 Procedure Option 1, the analysis is performed in terms of two parameters:

$$Kr = \frac{K_{Ia}}{K_{Ic}} \text{ ( or/and } Kr = \frac{K_{Ib}}{K_{Ic}}\text{)} \qquad \text{and} \qquad Sr = \frac{L}{Lc}$$

where $K_{Ia}$ and $K_{Ib}$ are the stress intensity factor (SIF) at the tip of crack semi-axes *a* and *b*, respectively, the crack being modeled by a surface emerging semi-elliptical material discontinuity. *L* is the applied loading on the involved element and $L_c$ is the limit load at plastic collapse. In the present analysis *L* is identified with the axial net stress $\sigma_x$ acting in the pressure vessel wall and $L_c$ is approximated by the material flow stress defined as $\sigma_{flow} = (UTS + YP)/2$. The principles of $K_{Ia}$ and $K_{Ib}$ calculation are outlined in [18].

With respect to residual stresses due to welding, their presence is attested by the fact that the crack developed in the weld joint area under the active action of the gas operating in the pressure vessel. This is a typical case of synergic effect of environment and stress induced cracking. Since the vessel has been subjected to a stress relief heat treatment after welding, only the amount of stress that has not been relaxed during the heat treatment will be considered in the analysis, additionally to the applied stress. Usually, it is accepted that welding residual stresses still acting after stress relief heat treatment amounts some 30 to 40% of initial peak residual stress which, as a rule, is in the range of yield point. Hence, a stress concentration factor (SCF) related to tensile residual stresses has been calculated, as follows:

$$SCF = \frac{\sigma_{\max}}{\sigma_x} = \frac{0.35 \times YP}{\sigma_x} = \frac{0.35 \times 359}{91.5} \cong 1.35$$

The tensile residual stresses are assumed to decay over a distance of approx. 25 % of wall thickness, i.e. over a distance 30 mm.

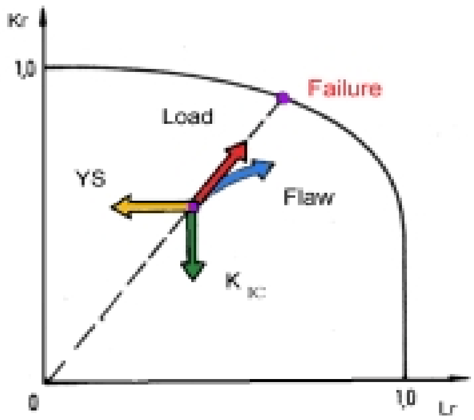


Figure: The effect of a increase of one of the paramerters, Yield Strength, Fracture Toughness $K_{IC}$, Load or Crack size in the Fracture Assessment Diagram FAD

## Deterministic failure risk assessment

Computer simulation of failure risk according to R6, Opt.1 Procedure has been made with the following input data:

| | |
|---|---|
| Material: | UTS = 460 MPa; YP = 359 MPa; Kc = 60 MPam$^{1/2}$ |
| PV geometry: | WT = 117 mm; IR = 1350 mm; b = 7 mm; 2a = 83 mm |
| Residual stresses: | SCF = 1.35; Decay length = 30 mm |
| Pressure: | $P_d$ = 152 bar (design pressure) |

The mean stresses acting in the PV wall are: $\sigma_h = 183 MPa$ (hoop) and $\sigma_x = 91.5 MPa$ (axial).

SIF values are: $K_{Ia}$ = 10.44 MPa m$^{1/2}$ and $K_{Ib}$ = 20.02 MPa m$^{1/2}$.

The figure below shows the representative state points in FAD diagram. Red point represents the state at the tip of *b* axis (maximum crack depth) and the blue one is related to the tip of *a* axis (tip of the crack on the inner face of PV). The red and green curves stand for Dugdale and R6 Opt.1 limiting curves at failure [17] . The counter in the lower left area of the display highlights the values of $K_{ra}$, $K_{rb}$ and $S_r$ parameters. Safety indices are also calculated as the ratio of the distance from the origin to representative point, to the distance, on the same path, from origin up to the limiting curve. Safety indices of 2.72 and 4.05 results as related to the crack depth (axis *b*) and crack tip on the inner face (axis *a*), respectively

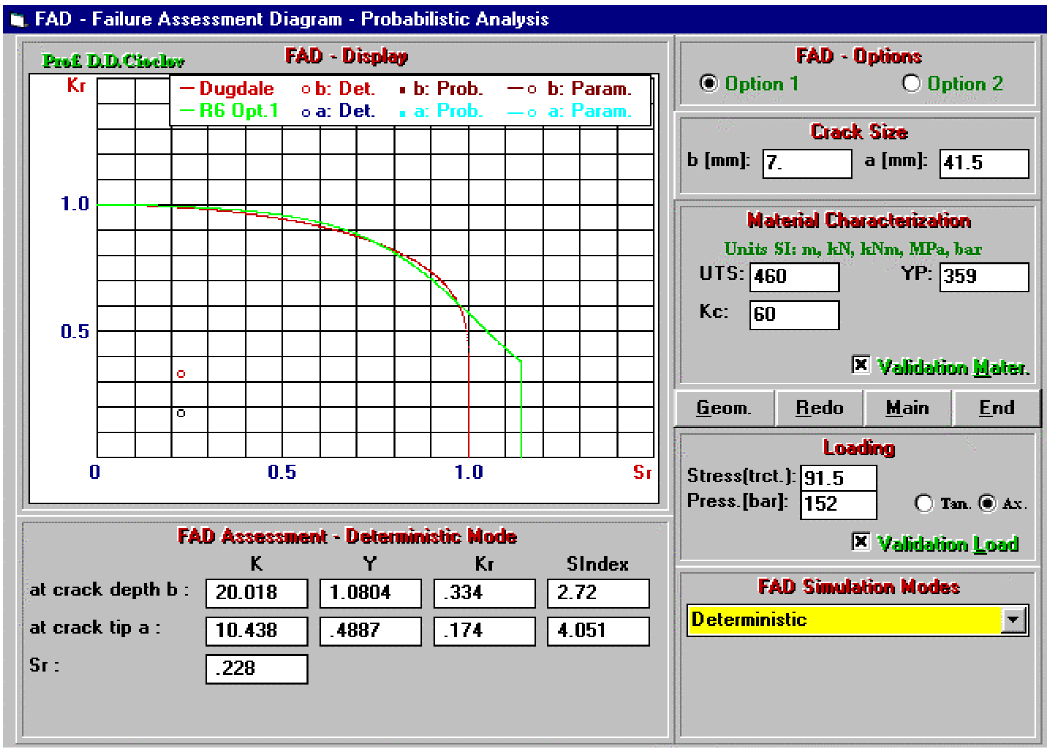


The calculation can be used to calculate the critical value that leads to immediate failure, if the other parameters were kept constant. With the assumed material and operational conditions, a crack size of 48.4 mm depth and 2×287 mm length on the inner face would lead to fracture (the crack aspect ratio i.e. **b/a** has been assumed constant) would lead to immediate failure.

A similar parametric analysis has been performed for material fracture toughness $K_c$. If a failure was due to insufficient fracture toughness, a critically low value of 20 MPam$^{1/2}$ would be required. The value used in the analysis is already conservertive and low. The Analysis can also be used to answer the question at what pressure, given the other conditions, the vessel would fail. The value would be 418.8 bar internal pressure.

It can be concluded that no danger of immediate failure exists. However, care must be exercised regarding the uncertainty involved in the choice of material strength and toughness characteristics together with the intrinsic uncertainty associated with NDT evaluation. In order to highlights this problem a probabilistic simulation of failure risk has been further attempted. A statistical (i.e. random) variation of crack size and material strength and fracture mechanics characteristics is assumed in this analysis.

**Probabilistic Failure Risk Simulation (PFRS)**

The principles underlying PFRS are: The uncertainty or random variation of a considered quantity (e.g. UTS, YP, Kc or *a* and *b*) is assumed to be described by a certain type of statistical distribution. The defining parameters of the distribution, such as mean value and standard deviation (SD) in the case of Normal distribution, are *a priori* fixed according to previous experience or expert opinion.

According to the assumed statistical distribution, a Monte-Carlo algorithm ("Monte-Carlo engine") generates, on computer, synthetic random values of the considered quantities.

The set of random quantities generated in one scenario (e.g. UTS, …, *a, b*) are introduced in a FAD analysis. A great number of scenarios are repeated. The probability of failure, $P_f$ is approximated by the ratio of the number of attempts that indicate failure to the total number of attempts. Several PFRSs has been performed.

This probabilistic analysis has been performed for a variation of crack size, variation in material strength and fracture toughness characteristics and a combination of both. Usually material strength and fracture toughness characteristics variation is regarded as a random variable described by a 3-parameters Weibull distribution. The generic analytical form of this distribution is:

$$\Pr ob(\arg ument < x) = 1 - \exp[-(\frac{x - x_0}{x_a - x_0})^w] \qquad \text{argument} \Rightarrow x_0$$

where $x_0$ is the inferior threshold, $x_a$ the scale parameter and $w$ the shape parameter. Specific parameters used in the probabilistic simulation are given in the table below

**Table** - Parameters of Strength and Fracture Toughness Weibull Distribution

| Random Variable | $x_0$ | $x_a$ | $W$ |
|---|---|---|---|
| UTS [MPa] | 440 | 485 | 2 |
| YP [MPa] | 340 | 385 | 2 |
| Kc [MPam$^{1/2}$] | 40 | 100 | 4 |

10,000 simulation have been performed. The FAD screen below illustrates the result of simulation. The result indicates a nil probability of failure. The representative points "cloud" is more disperse as in previous cases being, nevertheless, located well bellow the limiting failure curves.

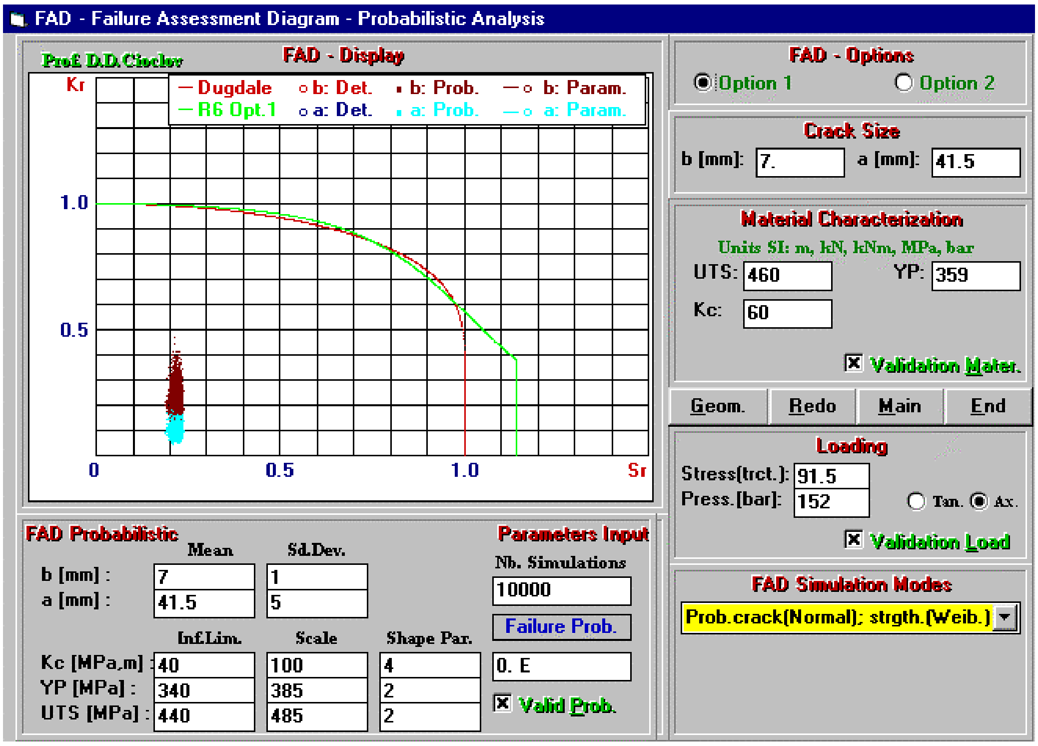


In this stage of analysis it may be concluded that in comparison with deterministic failure risk analysis, the probabilistic one gives a measure of how various uncertainty sources may shift the representation in FAD. It can be inferred from the results of probabilistic simulation that for normally encountered uncertainty in NDT crack detection, together with the uncertainty in the knowledge of material strength and fracture toughness characteristics and their inherent scatter, the representative points of the PV state in FAD are placed in the non-failure domain, well apart from the boundary to failure domain.

It must, however, be emphasized that the crack under analysis has developed as a typical environmentally promoted crack. It follows that the crack growth is a continuous process, a fact observed experimentally and explained in this case by the current values of SIF at both tips of the crack. Obviously, in the present state of the ammonia converter $K_{Ia}$ and $K_{Ib}$ are greater than a threshold SIF value $K_{th}$ that can be placed for a hydrogenous environment at as low values as 2 to 4 MPam$^{1/2}$ .

Bearing these facts in mind, it is vital to have now an estimate of the potential of crack growth under continuous operation and evaluate the increase of failure risk with time. Based on such an evaluation rationale time periods between two successive NDT inspections, repairs or even shutdown terms can be ascertained. This issue will be addressed in the next section.

## Estimation of Crack Growth Rate

Basic assumptions

The case under investigation, is subject to a environmentally assisted crack growth, where the crack extension occurs at virtually constant propagation rate. It is, however, common that when hydrogen is involved the crack growth rate (CGR), *dc/dt*, vs. maximum applied SIF assumes a trend as illustrated by the curve III in Fig. 3. This behavior can be modeled by a power type equation:

$$\frac{dc}{dt} = C(K_{\max}^{m} - K_{th}^{m}) \qquad\qquad K_{\max} \geq K_{th}$$

In this equation *c* stands for crack size on semi-axis *a* or *b*. *C* and *m* are empiric constants. $K_{th}$ is the lower threshold of SIF. For SIF lower than $K_{th}$ no crack growth occurs. In the range of SIF values near to *Kc,* the discrepancy between curve II and the observed behavior has little influence on overall crack growth estimation.

Estimation of crack growth parameters

For the purpose of the present analysis no appropriate data concerning *C, m* and $K_{th}$ values for the very specific environment prevailing in the ammonia reactor are known so far. One way of approach may be based on the interpretation of the limited amount of information on the crack growth as it is known after two successive sessions of NDT, with 35 days of separation. The crack situation is shown in the diagram. Considering that the crack growth along *a* axis was 8 mm during 35 days, i.e. 840 hours, and distributing this growth at the both surface crack tips, then a CGR can be estimated as

$$\frac{da}{dt} = \frac{0.008/2}{840} = 4.75\times10^{-6} \text{ [m/h]}$$

This *a* tip CPR was observed at an applied SIF of $K_{Ia}$ = 10.44 MPam$^{1/2}$. As far as the *b* crack tip (maximum crack depth) is concerned, no growth has been observed between the sessions. Conservatively, it will be further assumed that CPR along *b* axis (in depth) has the same value as along *a* axis the most exposed to the environment action. Under these suppositions the estimation of *C, m* and $K_{th}$ parameters is as follows:

$K_{th}$ value has been established at a conservative low value of 2 MPam$^{1/2}$. In the graph there is only one experimental available point ( 4.75.10$^{-6}$ ; 10.44) in the log(*dc/dt*) vs. log($K_{max}$) representation. Another point has been chosen accounting for a higher CPR of 2.10$^{-5}$ m/h at SIF limit $K_{max}$ = 60 MPam$^{1/2}$, in accordance with the increasing trend of variation, specific for crack growth in the presence of hydrogen. The following estimation has been obtained:

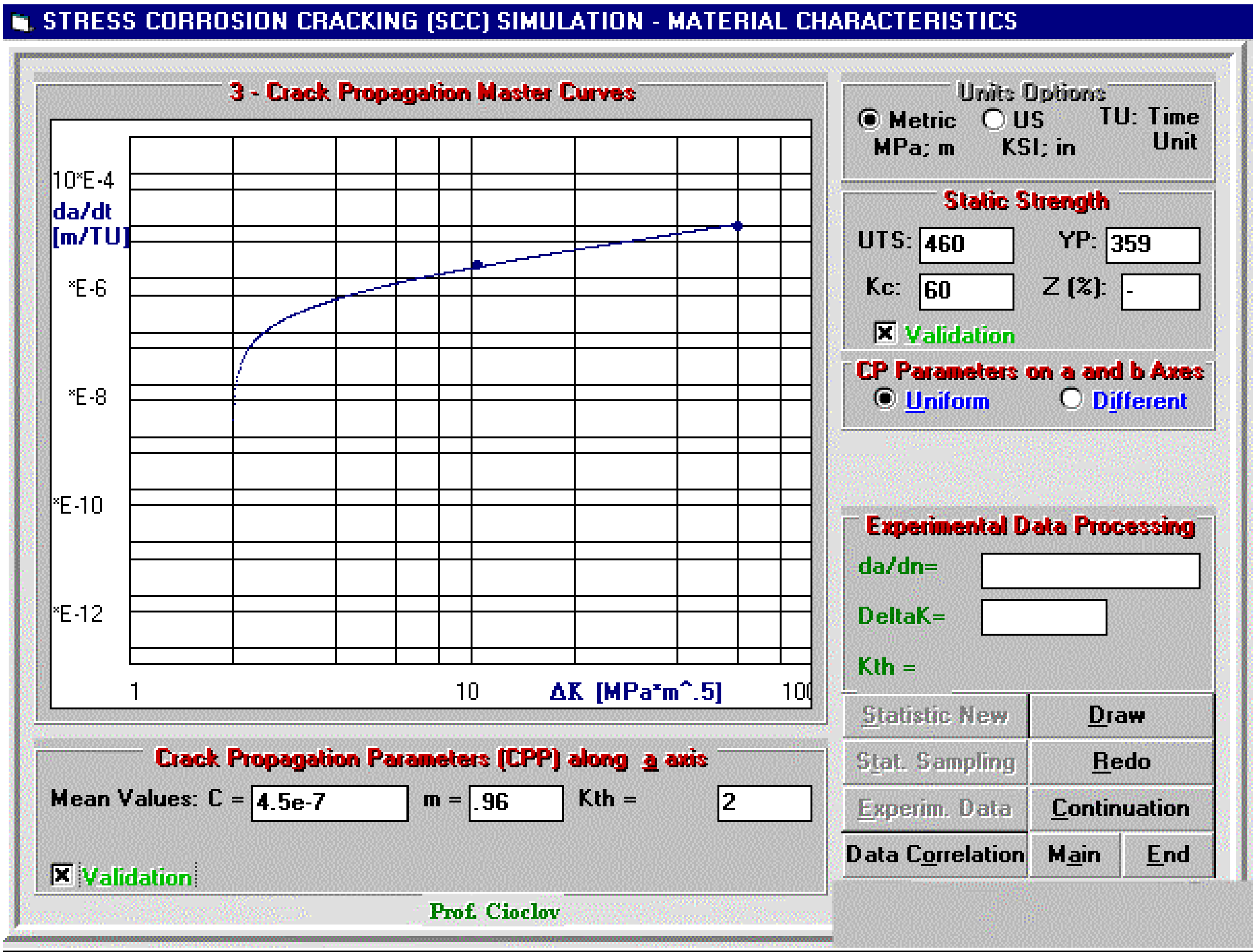


$C$ = 4.5.10$^{-7}$ [m/h]; m = 0.96; $K_{th}$ = 2 MPam$^{1/2}$

The result of crack growth simulation yields a time to failure of $t_f$ = 4970 hours.

## Estimation of NDT inspection interval

In order to establish a reliable time schedule for NDT inspection or PV repair, a way of approach similar to "safe life" philosophy, common in aerospace technology, has been considered. Accordingly, for a non-redundant load carrying structure, a factor of safety between 4 and 10 must be applied to the estimated PVs life, in order to substantiate an inspection time schedule. In the case under analysis the interval from the initial state to the next NDT inspection should be:

$$t_{NDT} = 4970/5 = 994 \text{ hours, i.e. } 41 \text{ days.}$$

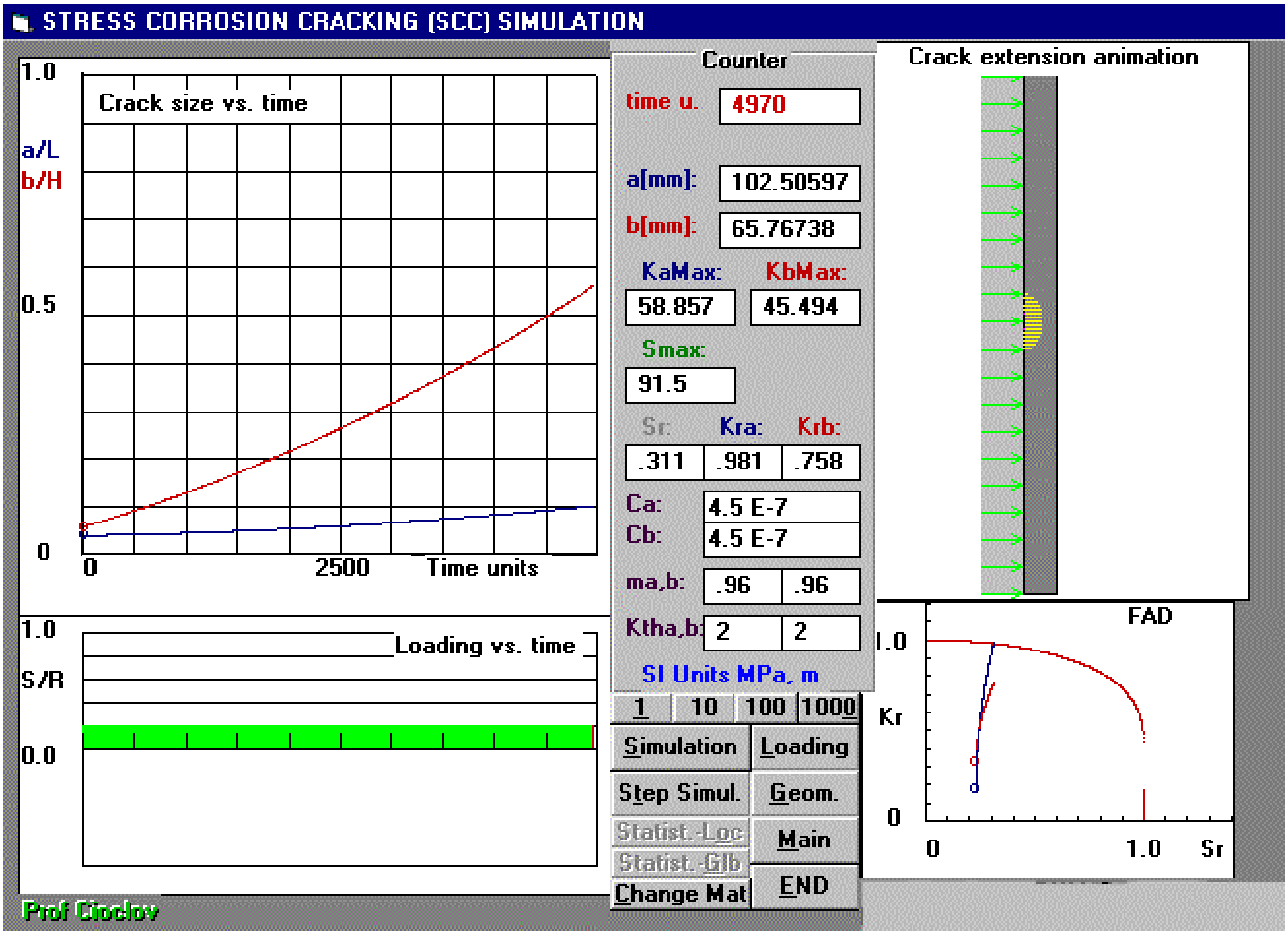


The above analysis contains some conservative assumptions related to:

- The low value of material fracture toughness used in the analysis that corresponds to the “worst case” situation, as results from the philosophy and data recommended by ASME Pressure Vessel Code, Sect. XI.
- In the crack growth model the input parameters account for crack growth at low stress intensity factors and accelerated growth at high SIF values.
- In order to evaluate the NDT time schedule a safety factor inspired by aerospace technology has been applied for the purpose of estimation of the remnant life of the PV.
- Conservative assumptions are related with SIF computation model, with due account of residual stresses that might be not have relaxed after stress relief treatment and with the implementation of sufficient scatter in computer probabilistic simulation of parameters that govern failure process.

The inspection interval was reestablished after every ultrasonic crack sizing.
Finally, the pressure vessel was repaired during a scheduled shut down.

4. Conclusion

Electromagnetic procedures are suitable for nondestructive evaluation of material degradation by embrittlement caused by copper-precipitates and neutron irradiation. Electromagnetic measuring methods have the potential for in-field embrittlement measurements. This way, electromagnetic predictive maintenance of power plant components can inform the provider about the current state of embrittlement.

Two new NDE approaches for the characterization of fatigue have been presented, namely the thermo-damping approach and the GMR–eddy current approach. The thermo-damping approach based on dissipated heat evaluation is suitable for fatigue damage characterization of Ti alloys. The GMR–eddy current approach based on a GMR technique is suitable for fatigue characterization in steels. Both approaches have proved their reliability in laboratory fatigue tests. However, their applicability on technical components has still to be confirmed.

So far a reliable crack sizing technique like the technique based on the detection of the crack-tip echo by using ultrasound can be applied, a quantitative NDE in combination with fracture mechanics becomes relevant so far a critical engineering assessment is an objective.

However, the NDE task of lifetime assessment today is of increasing interest because lifetime extension of components is asked for. In some countries for example, a lifetime of 60 years of a nuclear reactor pressure vessel is seriously discussed. The lifetime extension can only be performed on the base of a reliable and validated NDE. That's why European and internationally sponsored research programs [15] to the here discussed topics became popular.

**5. Acknowledgement**

We thank Donna Hurley and George Alers from NIST in Boulder, for their contributions concerning NDE of embrittlement and fatigue.

We also thank Karl-Heinz Katerbau and Siegfried Schmauder of the MPA Stuttgart, Germany, for mechanical hardness measurements and Monte Carlo simulation results.

**5. References**

[1] D. Willer, G. Zies, D. Kuppler, J. Föhl,. and K.-H. Katerbau, “Betriebsbedingte Eigenschaftsänderungen kupferhaltiger ferritischer Behälter- und Rohrleitungsbaustähle“, Reaktorsicherheitsforschung BMWi Förderkennzeichen 150 1087, *Final report October 2001.*

[2] J. Jansky, and G. Dobmann, “Indication of Creep Embrittlement in Low Carbon Steel Components using NDP-Methods”, in *12$^{th}$ Int. Conference* on *Structural Mechanics in Reactor Technology (SMiRT-12)*, Vol. G., edited by K.F. Kussmaul, Elsevier, Amsterdam, 1993, pp. 243-248.

[3] I. Altpeter, G. Dobmann, R. Kern and W.-A.Theiner, “Verfahren zur Erfassung thermisch induzierter Eigenspannungen mittels temperatur- und lastspannungsab-hängiger Barkhausenrauschmessungen“, Patent-Nr.: EU 95107743.7- 2204(1995).

[4] I. Altpeter, G. Dobmann, K.-H. Katerbau., M. Schick, P. Binkele, P. Kizler, and S. Schmauder, *Nuclear Engineering and Design* ***206***, 337-350 (2001).

[5] S. Schmauder, and P. Binkele, *Computational Materials Science (CMS)*, **24**, 42-53 (2002).

[6] I. Mc Henry, and G. A. Alers, “Nondestructive Characterization of Reactor Pressure Vessel Steels”, NRC Program RES-97-005, NIST Technical Note 1500-4, *Final Report June 1998.*

[7] G. Dobmann., I. Altpeter, R. Becker, R. Kern, U. Laub, and W.-A. Theiner, “Barkhausen Noise Measurements and Related Measurements in Ferromagnetic Materials“, in *Sensing for Materials Characterization, Processing and Manufacturing*,

edited by G. Birnbaum and B. A. Auld, Vol. 1, The American Society for Nondestructive Testing (ASNT), 1998, pp. 233-251.

[8] H. Rösner, S. Satish, and N. Meyendorf, "Nondestructive Characterization of Fatigue Damage with Thermography", in *Nondestructive Evaluation of Materials and Composites,* Conference Proceedings of SPIE Vol. 4336, New Port Beach, CA, 2001, pp.167-175.

[9] P. Grünberg, "Riesenmagnetowiderstand in magnetischen Schichtstrukturen", *Physikalische Blätter*, 51 (1995), pp.1077-1081

[10] G. Dobmann and M. Lang, "On-line Monitoring of Fatigue in the LCF and HCF range by using Micro-Magnetic NDT at Plain Carbon and Austenitic Stainless Steel", 8th ECNDT Conference proceedings, Barcelona, June 17-21, 2002, in CD-rom.

[11] G. Dobmann, "Early Fatigue Damage from the NDT-Point of View", in Review of Progress in QNDE, Vol.14, (D. O. Thompson, D. E. Chimenti, edit.), Plenum Press, New York, 1995, pp.2003-2010.

[12] U. Zerbst, C. Wiesner, M. Kocak, L. Hodulak, "SINTAP: Entwurf einer vereinheitlichten Europäischen Fehlerbewertungsprozedur – eine Einführung", GKSS Forschungszentrum, Geesthacht, Germany, 1999.

[13] D. D. Cioclov, M. Kröning, "Probabilistic Fracture Mechanics Approach to Pressure Vessel Reliability Evaluation", in *Probabilistic and Environmental Aspects of Fracture and Fatigue*, (S. Rahman, edit), The 1999 ASME Pressure vessel and Piping Conference, Boston, Massachusetts, August 1-5, 1999, pp. 115-125.

[14] H.-J. Schmidt, B. Schmidt-Brandecker, and G. Tober, "Design of Modern Aircraft Structure and the Role of NDT", Proceedings of the 7th ECNDT, Copenhagen, 26-29 May, 1998, Vol. 1, pp. 1-18.

[15] N. P. Aleshin, Project proposal #2378 of the International Science and Technology Centre (ISTC), "Development of techniques, equipment, and software to determine the remaining value (usability) of nuclear power plants, oil and gas pipelines, and other industrial installations", Moscow, 2002.

[16] Milne, I., Ainsworth, R.A., Dowling, A.R., and Stewart, A.T., Assessment of the Integrity of Structures Containing Defects. Central Electricity Generating Board, UK, Report R/H/R6-Rev3, May 1986.

[17] Marsdon, T.U., (editor) Flaw Evaluation Procedure: background and Application of ASME Section XI, Appendix A. EPRI NP-719-SR, Electrical Power Research Institute, Palo Alto, CA,1978.

[18] Newman, J.C., Raju, I.S., NASA Technical Memo. 85793, Langley Research Center, Hampton, Virginia, 1984.

[19] Cioclov, D. D., QNET/IZFP report, 1998